

## Micro-kinetics analysis based on partial reaction networks to compare catalysts performances for methane dry reforming reaction

Shambhawi; Weber, Jana M.; Lapkin, Alexei A.

**DOI**

[10.1016/j.cej.2023.143212](https://doi.org/10.1016/j.cej.2023.143212)

**Publication date**

2023

**Document Version**

Final published version

**Published in**

Chemical Engineering Journal

**Citation (APA)**

Shambhawi, Weber, J. M., & Lapkin, A. A. (2023). Micro-kinetics analysis based on partial reaction networks to compare catalysts performances for methane dry reforming reaction. *Chemical Engineering Journal*, 466, Article 143212. <https://doi.org/10.1016/j.cej.2023.143212>

**Important note**

To cite this publication, please use the final published version (if applicable). Please check the document version above.

**Copyright**

Other than for strictly personal use, it is not permitted to download, forward or distribute the text or part of it, without the consent of the author(s) and/or copyright holder(s), unless the work is under an open content license such as Creative Commons.

**Takedown policy**

Please contact us and provide details if you believe this document breaches copyrights. We will remove access to the work immediately and investigate your claim.



# Micro-kinetics analysis based on partial reaction networks to compare catalysts performances for methane dry reforming reaction

Shambhawi<sup>a</sup>, Jana M. Weber<sup>b</sup>, Alexei A. Lapkin<sup>a,c,\*</sup>

<sup>a</sup> Department of Chemical Engineering and Biotechnology, University of Cambridge, United Kingdom

<sup>b</sup> Intelligent Systems Department, Technische Universiteit Delft, Netherlands

<sup>c</sup> Cambridge Centre for Advanced Research and Education in Singapore (CARES Ltd), 1 Create Way, Singapore

## ARTICLE INFO

### Keywords:

CO<sub>2</sub> reforming of methane  
Reaction Network  
Catalyst design  
Heterogeneous catalysis  
Catalyst descriptors  
Network accumulation and congestion

## ABSTRACT

Designing a simple, yet representative reaction network for subsequent micro-kinetic analysis is important for limiting the cost of evaluation and ensuring model solvability. This is currently achieved by employing sensitivity analysis over a comprehensive reaction network (CRN) to screen reaction species. However, as a reaction network is being simplified for a particular catalyst composition, it loses its transferability to other compositions. Therefore, in this study, a two-way approach is presented to circumvent this problem. Firstly, a generalizable model outcome is identified, i.e. minimum reactant conversions ( $x_R$ ), based on a mass-flow analysis. Then, a stepwise workflow is developed for constructing a partial reaction network (PRN) to insure transferability of min ( $x_R$ ) for a range of varying catalyst energetics, in the absence of experimental data for validation. Lastly, the transferability of this approach is demonstrated for CH<sub>4</sub> dry reforming by developing a PRN using Ni(1 1 1) as the initial catalyst and testing it over Ru(001).

## 1. Introduction

If we had formal rules of heterogeneous catalyst design, these would be based on the knowledge of relevant reaction kinetics at the surface, identified through experimental observations and the construction of accurate micro-kinetic models. Here Micro-kinetic modelling (MKM) is a tool for theoretical investigations of catalysts performance: MKM inputs catalyst structure and outputs its performance for a given reaction in terms of the predicted reactant conversions and product yield. The method has gained significant popularity in the past decade, see Fig. 1 (a), because unlike traditional methods such as power – law expressions [1] and the Langmuir-Hinshelwood - Hougen-Watson (LHW) equations [2] that are often based on chemical intuition and implicit assumptions, the MKM method does not require any initial assumptions about the rate-determining reactions or the most abundant surface species [3].

Fig. 1(c) illustrates a generic strategy for developing a micro-kinetic model. It starts by (1) building a reaction network that includes possible reaction intermediates and elementary reaction steps based on experimental observations, literature-based dissociation and association routes, and/or auto-reaction generators algorithms [4] employing reaction energy data [5–7], templates [8,9] or heuristics, see Fig. 1(b). The

most common approach is to look in the literature for elementary steps corresponding to reactant dissociation, product association and redox reaction steps in similar reactions with known mechanisms. For example, a study on methane reforming [10] copies the mechanism for dry reforming of methane (DRM) directly from CH<sub>4</sub> steam reforming with the addition of CO<sub>2</sub> dissociation steps. Further comparisons show that for small molecules reaction systems like DRM, both literature and automated mechanism generators agree on the same reaction network [4,10]. Identifying a reasonably accurate and feasible reaction network is the first and critical step in micro-kinetic modelling as it directly affects (i) the cost of developing a model and (ii) its accuracy.

The next step, (2) is computing reaction energetics, i.e. intermediate binding energy and transition state barriers corresponding to the reaction network obtained in step (1) over a given catalyst surface using tools like density functional theory (DFT). This is followed by step (3), reactor modelling.

Mass balance equations are written for all reaction species (reactants, products and intermediates) in a given reactor system (e.g. a plug flow reactor) based on elementary reaction steps in the reaction network. Solving this set of mass-balance equations generates intermediate surface coverages, reactant conversions, product concentrations and reaction rates of elementary steps for a given reaction condition. These

\* Corresponding author at: Department of Chemical Engineering and Biotechnology, University of Cambridge, United Kingdom.

E-mail address: [aal35@cam.ac.uk](mailto:aal35@cam.ac.uk) (A.A. Lapkin).

<https://doi.org/10.1016/j.cej.2023.143212>

Received 20 February 2023; Received in revised form 4 April 2023; Accepted 24 April 2023

Available online 27 April 2023

1385-8947/© 2023 The Author(s). Published by Elsevier B.V. This is an open access article under the CC BY license (<http://creativecommons.org/licenses/by/4.0/>).

solutions are then compared to experimental data (4) to estimate model accuracy.

The accuracy of an MKM relies on its model parameters that are specific to each step shown in Fig. 1c. Loosely constrained kinetic models can lead to several pitfalls in terms of both accuracy and computational cost, and the results based on such models can lead to varying conclusions regarding the reaction mechanisms and catalyst performance [11]. Starting with reaction networks, the important parameter is the energy tolerance that is used to decide whether a particular intermediate/reaction step will be included in the reaction network. Similarly, in step (2), there is a significant impact of the choice of parameters corresponding to the quantum chemistry tool used for generating energetics. For example, in the case of DFT, it would be the exchange–correlation functional. In step (3), it is the approach used for mapping the catalyst surface (mean-field approximation [12] or kinetic Monte Carlo [13]). Another impact factor is whether assumptions of certain elementary reactions are in quasi-equilibrium had been used sparingly [14].

Several studies have been dedicated to ensuring the validity/applicability of these MKM parameters/assumptions in steps (2) and (3) of the overall methodology respectively. For example, DFT functionals were tested against experimentally observed energies for gas-phase molecules and catalyst bulk systems, before generating the entire surface energetics [15]. Also, error quantification of MKM predictions was performed to validate the use of linear scaling relations for predicting intermediate and transition state energies [16] to justify its application. There have also been studies that are more focused on generalization and transferability of MKM parameters instead of absolute prediction accuracy. A study in ref. [17] reports that catalysts performances can be directly compared if the same DFT functional is used to generate energetics over each catalyst surface, even when their absolute values are different from experimental observation. Similar investigations for mean field approximation validate its direct applicability to high-

temperature reaction systems [12]. Additionally, studies performing error quantification are used to differentiate specific scenarios that need complex models, like kinetic Monte Carlo instead of mean-field [17,18], thus enabling efficient resource allocation based on problem requirements. These findings eliminate the dependence on experimental data for tuning parameters or validating assumptions when comparing catalyst activity, i.e. materials can be categorised on whether or not they are more active than a base catalyst material. It is particularly useful since the general objective of micro-kinetic modelling is to enable catalyst design by comparing catalysts performances.

Additional investigation to establish guidelines for creating a representative reaction network (step 1 of Fig. 1c) and its generalization to model outcomes would significantly reduce the cost of constructing and validating MKMs. It will also broaden the scope of independent theoretical investigations in guiding experiments, rather than the other way. Reaction networks directly impact the computational cost and prediction accuracy further down the line.

Ideally, a reaction network should include all possible elementary surface reactions occurring during the catalytic transformation of reactants to products, i.e. a comprehensive reaction network (CRN). However, this process of developing a CRN is based on existing studies, i.e. a CRN is a superset of reaction steps reported in the literature. As a result, CRN models are computationally expensive and often include high numbers of surface variables making them unsolvable [4]. They might also include intermediates/reaction steps whose absence has a negligible effect on the model outcome. Therefore, in practice, models are developed over partial reaction networks (PRNs) that are created by screening relevant intermediates and reaction steps, from a comprehensive network.

Screening PRN from CRN is often based on intermediate binding energies and transition state barriers. Sensitivity analysis is performed over the micro-kinetic model to identify transition states and intermediate binding energies that dominate the reaction kinetics followed by

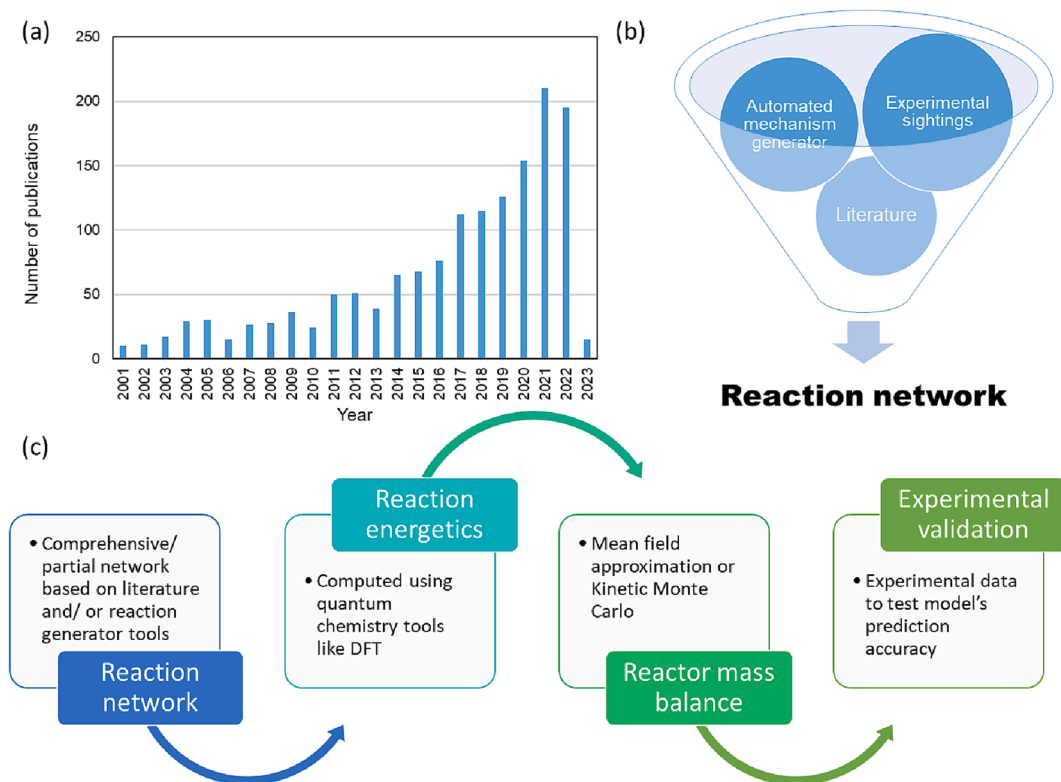


**Fig. 1.** The role of microkinetic modelling in catalysts development. (a) Publications appearing in the Web of Science search (as of February 8, 2023) for the term “Micro-kinetic modelling”. (b) The sources of data used in constructing a reaction network.[4] (c) Illustration of a stepwise strategy for developing a micro-kinetic model.

mechanistic insights into the reaction. Many studies [19–21] employ dimensionality reduction methods like principal component analysis (PCA) based on sensitivity coefficients of each reaction step in a CRN to create a reduced model. Whereas, some studies [19–22] are dedicated to identifying universal descriptors for a reaction system i.e., binding energies and activation barriers corresponding to kinetically relevant reaction steps, e.g. degree of rate control [23]. These identified descriptors are the basis for developing tools like machine learning-based binding energy prediction models [24] for cost-effective screening of catalytic materials. The entire process is a theoretically guided catalyst design approach that employs micro-kinetic models ideally built using a simple and transferable PRN.

In reality, simplicity and transferability are contradictory properties of a PRN that needs to be optimized for a given reaction system. Screening of either intermediates or reaction steps depends on the catalyst's bulk composition and reaction conditions in question. The bulk components directly affect the binding energy, whereas reaction conditions, such as elevated temperature/pressure, might activate certain pathways that were previously dormant. For example, a study on CO<sub>2</sub> methanation revealed that the intermediate HCOO\* is among the most abundant intermediate species on Ru (001) but the same is not observed for Ni (111) [25]. It is also noted that reaction steps like the Boudouard reaction become relevant at temperatures above 800 K but are dormant at lower temperatures [26]. Therefore, the transferability of a reaction network is only confirmed after validating the corresponding model predictions against experimental findings performed over similar catalyst bulk compositions and reaction conditions, step (4) in Fig. 1c. This requirement for validity, however, limits the direct application of PRN-based models, and descriptors by extension, as a tool for faster theoretical investigation of catalysts.

Direct comparisons of catalysts performance are only valid if: (i) model transferability is proven experimentally over every catalytic system in question, or (ii) transferability of model parameters in steps (1), (2) and (3) illustrated in Fig. 1c is justified based on generalizations available in the literature. The latter has already been investigated for steps (2) and (3), as we discussed above. Therefore, in this study, we establish guidelines on the construction and use of single pathway PRNs (reaction networks comprising of one pathway that allows product formation from reactants) for catalysts comparisons while ensuring transferability. We particularly focus on reaction systems allowing

atmospheric CO<sub>2</sub> capture (a reference to Section 2.1), such as dry reforming of methane (DRM) and CO<sub>2</sub> methanation. Both are simple molecular chemistries that favour carbon capture and have extensive literature devoted to identifying active and stable catalysts *via* micro-kinetic analysis. We use DRM as our test reaction system for developing a single pathway PRN and then compare its results to a previously validated CRN on different Ni-based catalyst surfaces for the CH<sub>4</sub> dry reforming.

The results of this investigation are reported in Sections 3.1 and 3.4. We also present a mass flow analogy based on this comparison in Sections 3.2 and 3.3. We then identify model outcomes that can be generalized over different catalyst surfaces in Section 3.5 and test them for certain binding energy constraints in Section 3.6. We also outline those constraints and devise a workflow in Sections 3.6 and 3.7 to construct a transferable PRN, i.e. a 'bare-minimum' partial reaction network that allows catalyst activity comparisons based on reactant conversions using micro-kinetic model predictions in the presence of limited or no experimental data to ensure its transferability. We then examine the workflow applicability for stiff systems like CO<sub>2</sub> methanation later in Section 3.7.

## 2. Methodology

Fig. 2 outlines the methods used in this study to compare predictions from models based on CRN and PRN that are later used to develop guidelines for developing a transferable PRN. Computational details for constructing partial/comprehensive reaction networks and micro-kinetic modelling are discussed in Sections 2.1 and 2.3 respectively. The DRM reaction model is first employed over different Ni-based catalysts to compare their respective PRN and CRN model outcomes. It is then employed on a set of hypothetical Ni-based catalysts and another set of random catalysts. The technique for developing hypothetical Ni-based catalysts and random catalysts is reported in Section 2.2.

### 2.1. Reaction networks

Reactions of DRM and CO<sub>2</sub> methanation have been extensively studied in the literature. Experimental studies employing isotopic tracing [27–29] indicate the presence of intermediates like surface carbon (denoted as C\*) and surface CO (CO\*) on Ni-based catalysts. Further analyses using Fourier-transform infrared spectroscopy (FTIR)

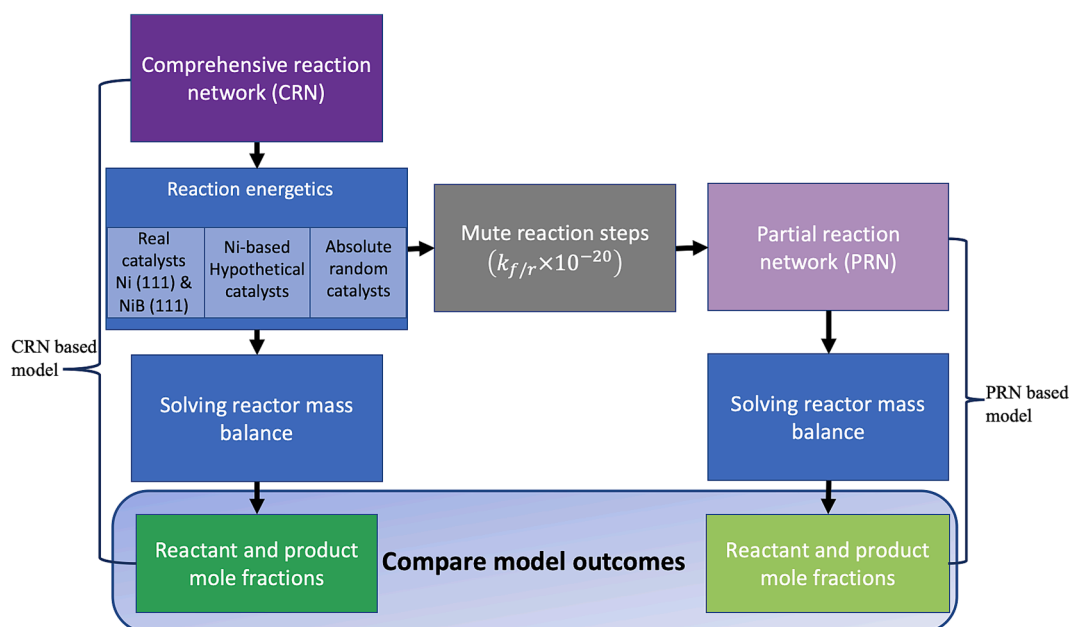


Fig. 2. A summary of methods for comparing models based on comprehensive reaction network (CRN) and partial reaction network (PRN).

suggest the presence of formic and formaldehyde intermediates [30,31]. These findings are included in theoretical investigations. However, independent studies report different reaction networks, varying from the most comprehensive reaction networks, for example including both formic and aldehyde species [25,26] to a generic partial reaction network [32,33], or ignoring formic species. Please refer to Table S1 in Supporting Information (SI) for further details.

The CRNs constructed in this study are based on the recent comprehensive studies for DRM [26] and CO<sub>2</sub> methanation [25] respectively. Please refer to Fig. 3 for the CNR corresponding to the dry reforming reaction. It includes all side reactions, such as H<sub>2</sub>O formation, Boudouard reaction, water gas shift (<800 K) and reverse water gas shift (>800 K) reactions. The CRNs for DRM and CO<sub>2</sub> methanation, consist of 38 and 46 elementary reaction steps respectively (reactions listed in Table S2 of SI, please refer to refs. [26;25] for further details). The binding and transition state energies of the reaction network are taken from previous studies [25,26]. This CRN is represented as two connected graphs to investigate the connectivity between the intermediates. The nodes correspond to reaction intermediates and the edges correspond to each elementary reaction step (including both forward and backward reaction steps). Please refer to Section 2 in SI for further details on the visual representation of chemical reaction networks.

PRNs, on the other hand (Fig. 4), are created by muting certain reaction steps in the CRNs. The reaction steps are muted by multiplying their rate constant by a factor as low as 10<sup>-20</sup>. For PRN-1, the reaction steps that are not included in the dominant pathway (for product formation over Ni (111)) and side reactions, are muted. A model is then developed based on PRN-1 and its model outcomes are compared against the CRN-based model for Ni-based real catalysts and hypothetical catalysts, (please refer to Section 2.2 for more details). The relevance of side reactions is also investigated similarly, i.e. by muting side reactions and comparing the model outcomes with CRN-model, please refer to Section 6 of Supporting Information (SI) for details.

Mass flow within such chemical reaction networks (Figs. 3 and 4) provides a new perspective to approaching kinetic analysis of catalysts. The rate of mass flow/accumulation through the networks are known indicator of catalysts' performance and it is dependent on: (i) the

catalyst's energy profile in the specific reaction, and (ii) the reaction graph's topology. Preliminary studies on reaction networks report that mass flow in reaction network topologies with multiple pathways could be prone to 'congestion' – a network property [34]. Similarly, lower binding energies of intermediates might lead to mass accumulation and further catalyst poisoning (a reference to Section 3.5). These reports are quite relevant since both DRM and CO<sub>2</sub> methanation support the existence of multiple intermediates and pathways: according to the pathway identification technique based on Dijkstra's algorithm [25], there are 835 unique pathways for CO formation from CH<sub>4</sub> in DRM and 5,515 pathways for CH<sub>4</sub> formation from CO<sub>2</sub> in the CO<sub>2</sub> methanation network.

For such reaction networks, congestion/accumulation is an inter-linked phenomenon whose extent is affected by both energetics and connectivity, (i.e. network topology). This requires an additional investigation to enable the study the phenomena of congestion and accumulation separately. An absolute random catalyst (ARC) is created that favours all reaction steps equally and ensures congestion in the networks with interlinked pathways (please refer to Section 2.2 for more details). Then a multi-pathway network, i.e. PRN-2 (Fig. 4b), is created that includes every intermediate listed in CRN to mimic its extent of accumulation. However, it only includes three independent pathways leading to product formation. Hence the difference in model outcomes from PRN-2 and CRN-based MKMs (see Fig. 2) will be the result of network congestion observed in CRN. Similarly, PRN-1/ARC-based models are also compared against the CRN/ARC-based model to understand the impacts of congestion and accumulation phenomena when occurring together.

## 2.2. Energetics for random catalysts

Random catalysts are created in two ways: (i) an absolute random catalyst (ARC), and (ii) a Ni-based hypothetical catalyst (NiHC). ARC is designed to favour all reaction steps in the CRN or a DRM equally. The forward rate constants of all 38 reaction steps are set to 10 s<sup>-1</sup> and backward reaction steps are set to 5 s<sup>-1</sup>. On the other hand, the NiHC is designed to mimic a real catalyst' potential energy surface (Equations 1–2). The reaction energies for this case were assigned by overlapping

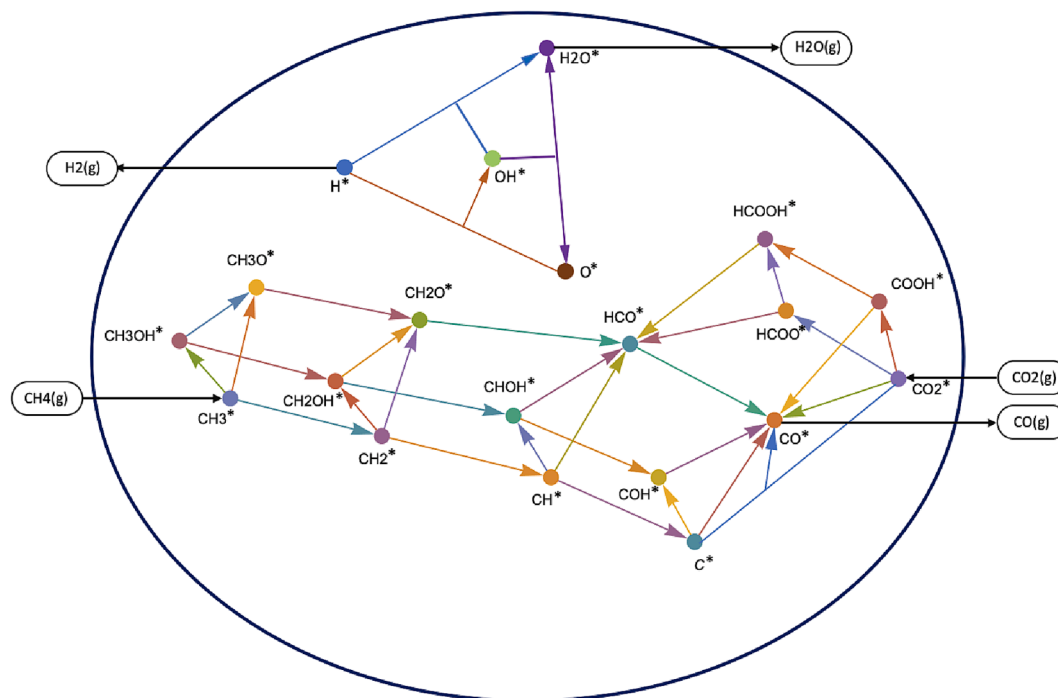
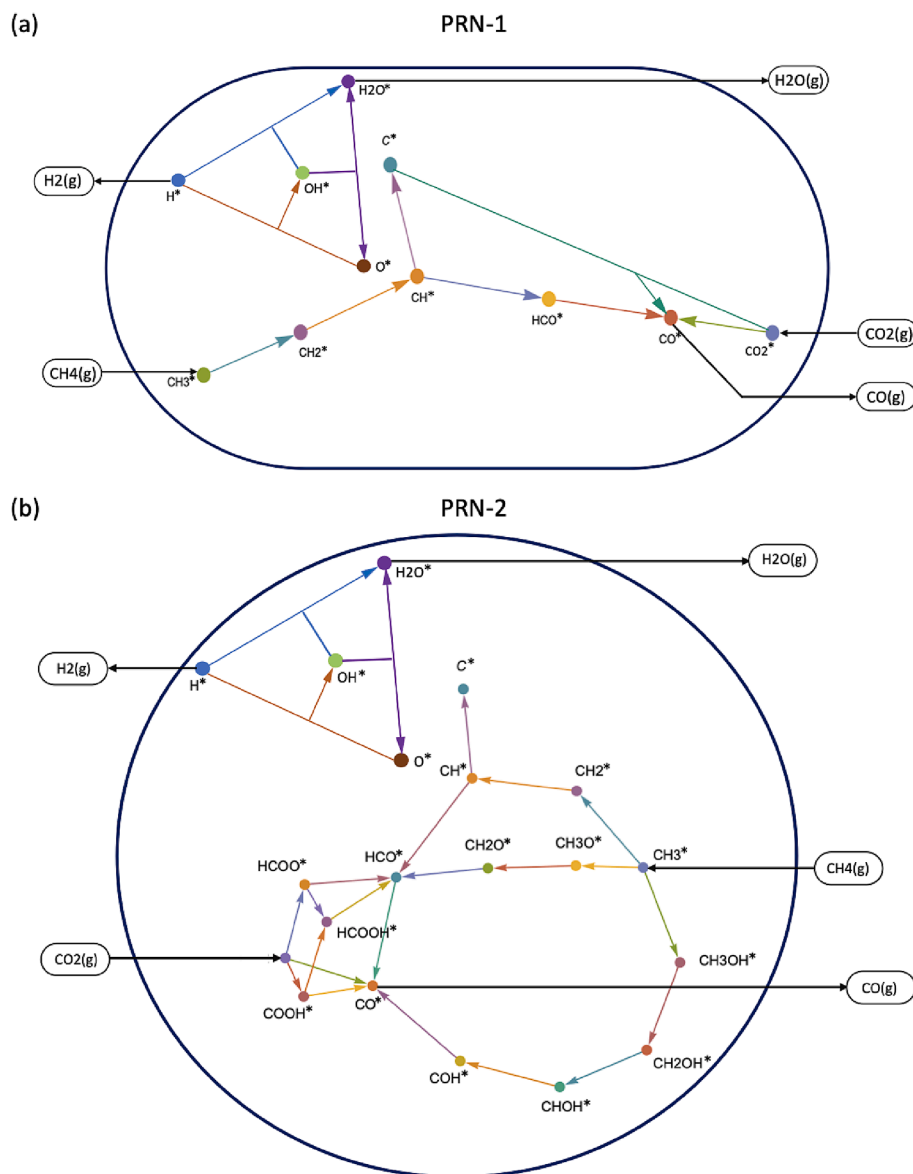


Fig. 3. A comprehensive reaction network (CRN)[26] for dry reforming of methane. Nodes correspond to reaction intermediates and edges correspond to each elementary reaction step. For simplicity, only the forward reaction steps are shown in this representation.



**Fig. 4.** Illustration of network connectivity in the designed partial networks. (a) PRN-1 for dry reforming of methane constructed using the dominant pathway identified over Ni(111) catalyst [26] at 973 K / 10 bar and reactor space-time of 1 gcat h mol<sup>-1</sup>. (b) PRN-2 for dry reforming of methane that includes multiple independent pathways for product formation and all intermediates listed in the comprehensive reaction network (CRN).

the Ni potential energy surface with a random energy surface with lower and upper bounds of 50 kJ mol<sup>-1</sup>. The bounds were later increased to 100 kJ mol<sup>-1</sup> for further investigating the effect of reaction energies on partial network predictions, see Section 3.6.

$$E_{a,j} \geq 0 \quad (1)$$

$$E_{a,j} \geq \Delta H_j \quad (2)$$

where  $E_{a,j}$  and  $\Delta H_j$  are the activation barrier and reaction energy for  $j^{\text{th}}$  the reaction step respectively. Scaling relation and BEP relation constraints (see Equation 3–5) are included in addition to the constraint in Equations (1), (2).

$$\Delta E^{ZH_x} = \gamma(x)\Delta E^Z + \varepsilon \quad (3)$$

where,  $\Delta E^{ZH_x}$  is the adsorption energy of the species  $ZH_x$  ( $Z = \text{C}, \text{N}, \text{O}, \text{S}$ ) on the most stable site,  $\Delta E^Z$  is the adsorption energy of the species  $Z$  at the same site [35],  $\gamma(x)$  is the slope in equation (3) computed using to the remaining valency of the bonding atom ( $Z$ ) and intercept  $\varepsilon$  is a constant

depending on the site configuration [35,36].

$$E_{a,j} = \alpha \Delta E_{FS/IS,j} + \varepsilon \quad (4)$$

$$-2 \leq \gamma(x), \alpha \leq 2 \quad (5)$$

Changes in transition state energies ( $E_{a,j}$ ) are linearly related to the changes in intermediate binding energies in initial/final states ( $\Delta E_{FS/IS,j}$ ) of any  $j^{\text{th}}$  reaction, which in turn is linearly related to the binding energy changes of atomic carbon and oxygen. The upper and lower bounds for slopes in Equation 3–4 are 2 and -2 respectively. These bounds are based on the ranges of slope values observed in the literature for multi-metallic alloys [37]. The intercept, on the other hand, is the same for all catalysts since the same planar surface is investigated. As a result, intercepts do not amount to any changes in the binding energy when compared against the Ni(111) surface and can be ignored.

The random energies are generated using MATLAB's random number generator. Reaction energies that satisfied the constraints of Equation 1–5 were identified using MATLAB's functions createOptimProblem, list and RandomStartPointSet.

### 2.3. Micro-kinetic analysis

The simulations are based on the previously reported model for DRM and CO<sub>2</sub> methanation over Ni(111) surface [25]. The rate constants for

each elementary reaction step are obtained using transition state theory, Equation (6).

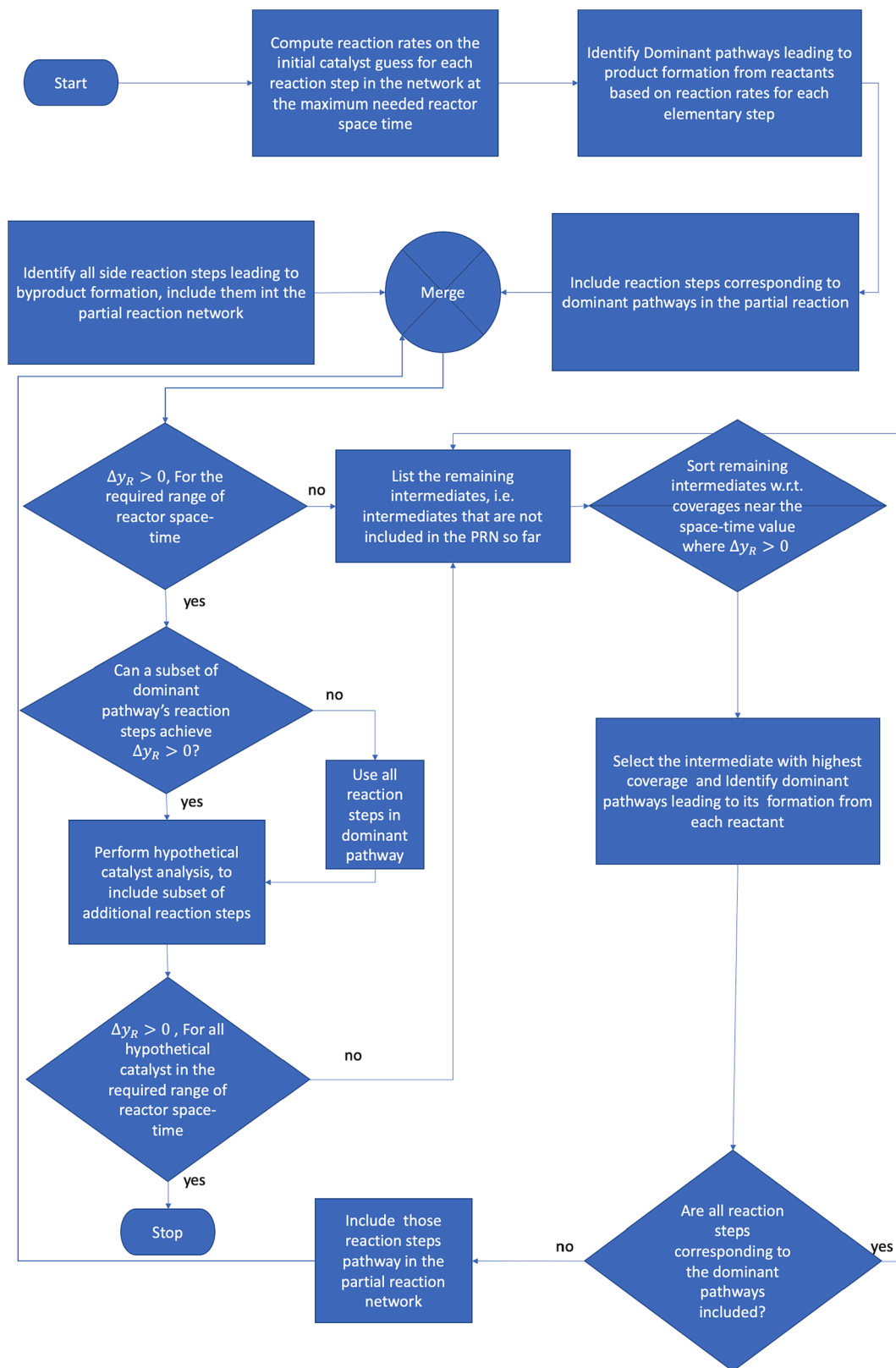


**Fig. 5.** An illustration of the generic workflow for constructing a partial reaction network (PRN) for estimating minimum reaction conversions based on an initial catalyst guess and a range of reaction conditions.

$$k_f = k_B T/h \exp\left[\frac{-\Delta G_{act,f}}{RT}\right] \quad (6)$$

where  $k_B$  is Boltzmann constant,  $h$  is Planck's constant,  $R$  is the universal gas constant,  $T$  is the reaction temperature and  $\Delta G_{act}$  is Gibbs free energy of activation for the reaction step obtained from DFT values.  $\Delta G_{act}$  for each elementary reaction step is taken directly from previous the study.



$$r_f = (k_f \theta_A \theta_B) \times N_{site, total} \quad (7)$$

Once rate constants are computed using Equation (6), the forward and backward rates ( $r_{f/b}$ ) are given as Equation (7). Here  $\theta_A$  and  $\theta_B$  are the fractional coverages or mole fractions of species  $A$  and  $B$ , and  $N_{site, total}$  is the total number of active sites in mol/g<sub>cat</sub>.

The rate equations are then assembled based on the mass balance equations for each species. Considering an ideal PFR reactor as a reasonable simplification for a typical fixed-bed reactor, the reactants conversions are written in the form of differential equations of reactants balances (Equation 8). The micro-kinetic model (MKM) is developed assuming the mean field approximation. A detailed list of assumptions can be found in the reported studies [25,26].

$$\frac{d\theta_j}{d\left(\frac{W}{F_0}\right)} = \sum_i^{\#of reactions} \sigma_{i,j} r_i \quad (8)$$

where,  $W$  is the weight of the catalyst in g,  $F_0$  is the total molar flow rate of gases in mol•h<sup>-1</sup>,  $\sigma_{i,j}$  is the stoichiometric coefficient of species  $j$  in reaction  $i$ ,  $r_i$  is the rate of reaction  $i$  and  $\theta_j$  is the fractional surface coverage of surface species  $j$  or mole fraction of gas phase species.

The micro-kinetic model is solved for a reaction temperature/pressure of 973 K / 10 bar pressure for DRM and 550 K / 10 bar for CO<sub>2</sub> methanation. The reactor space-time ( $\frac{W}{F_0}$ ) is varied up to 1 g<sub>cat</sub>•h mol<sup>-1</sup> and Mathematica's NDSolve is used for solving mass balance ODEs. To eliminate stiff solutions arising due to Mathematica's high accuracy (10<sup>-15</sup>), the model predictions rounded to five decimal places, please refer to Section 7 in SI for further details.

Subsequent analysis for identifying rate-determining step (RDS) and the dominant pathway is also performed. Rates are computed for each reaction step in the network and pathways are listed using the pathway identification algorithm [25]. For a given pathway, the reaction step with the smallest reaction rate is its RDS. The pathway with a maximum rate of RDS is identified as the dominant pathway. Please refer to ref. [25] for further details.

### 3. Results and discussion

This section highlights the major results of this study, i.e. guidelines for developing representative and transferable partial reaction networks (see Fig. 5) for catalyst screening and relative comparisons while circumventing the computational bottleneck that limits the applicability of MKMs. These guidelines can be directly implemented to problems dealing with prediction of catalysts activity and optimisation of reactant's conversions by modifying catalyst composition.

For a given set of reaction conditions, initial catalyst guesses and a range of reactor space-time, a partial network must be constructed such that:

- Intermediates corresponding to the dominant pathway for product formation at the maximum reactor space-time on the initial catalyst guess are included.
- All by-products and side reactions are identified, as per the reaction thermodynamics, and included (to account for reactant mass diversion away from product formation).

- Most abundant intermediates that are not part of the dominant pathway are also identified over the initial catalyst for the given space-time and included (to account for mass-flow accumulation of oxidizing agents and catalyst poisoning).
- Step (c) is repeated for a range of reaction energies using the hypothetical catalyst analysis as mentioned in Section 3.6. The relevant intermediates identified through this analysis are included in the network (to account for possible mass accumulation due to changes in energetics).
- All reaction steps corresponding to the dominant pathway for the formation of a relevant intermediate identified in Steps (c) and (d) are noted (to account for minimum reactant conversion).
- Different subset of the reaction steps added in Step (e) are tested for minimum reactant conversion of PRN and only the smallest subset is included.

These guidelines are developed after thoroughly examining the effects of reaction network topology and energetics towards different model outcomes, i.e. reactant and product mole fractions. In Section 3.1, the reaction topology is investigated by comparing reactant and product mole fractions obtained from CRN and PRN-based models for a given catalyst energetics. In Section 3.2, the mass-flow analogy is used to project catalyst performance in terms of flow congestion and accumulation. This flow analogy is further used in Sections 3.3-3.4 to understand the results of network comparison in previous sections. Additionally, the energetics is also varied in Sections 3.5-3.6 by employing ARCs and NiHCs to investigate the generalizability of model outcomes when using PRNs. Lastly, the transferability of this workflow is tested in Section 3.7.

#### 3.1. Comparing model predictions for varying reaction networks

The construction of a representative reaction network is the most important step towards micro-kinetic modelling. Different reaction networks, like DRM's PRN-1 and the CRN in Figs. 3 and 4, can result into different model outcomes, see Figs. 6-8. Thus, questioning the transferability of absolute model predictions over different catalysts, even if they are just slight modifications of each other. For example, PRN-1, that is constructed using Ni(111) as the initial catalyst, does not provide accurate absolute predictions for B-doped Ni(111) surface and Ni-based hypothetical catalyst. This difference is found to be higher at smaller reaction space-times.

From Figs. 6-8, it is observed that the absolute predictions of CRN- and PRN-based models vary depending on the catalyst surface, i.e. Over the Ni(111) surface, the CRN and PRN model predictions are coinciding, whereas for the NiB(111) and the NiHC catalyst, the predictions differ significantly. This is due to the fact that the PRN-1 model includes the dominant pathway observed over Ni(111) surface, while that is not the case for other catalysts.

It is found that the absolute predictions of the PRNs-based models are only reliable when all elementary steps corresponding to the pathways significantly contributing to product formation are accurately identified and included. The CRN-based model predicts a 14.7% contribution of the dominant pathway (or PRN-1) towards product formation on Ni(111) at a reactor space-time of 1 g<sub>cat</sub>•h mol<sup>-1</sup>, whereas the contribution of the same pathway over NiB and NiHC is 0.005% and 2.7% respectively. However, if PRNs are created using dominant pathways identified over NiB(111) and NiHC (please refer to Table S3 in SI) and implemented respectively, then their absolute model predictions (Figures S2 and S3 in SI) are coinciding with the CRN predictions just like Fig. 6. Despite such observations, PRNs are often used in literature for reporting conversions and yield over different catalysts, without validating their network to every catalyst system in the study [38,39]. Thus, are the resulting varying mechanistic insights and catalyst performance predictions across literature.

Regardless of the limited transferability of absolute PRN predictions,

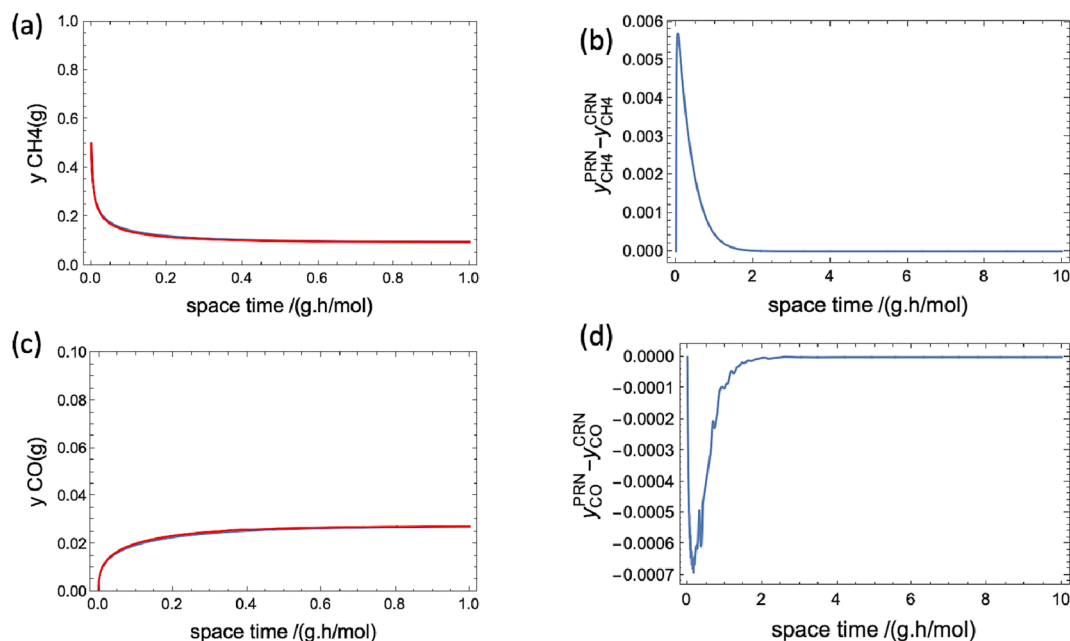


**Fig. 6.** Model predictions of (a) reactant (CH<sub>4</sub>) mole fraction when using the comprehensive reaction network (CRN) (red) vs the partial reaction network (PRN) (blue), (b)  $\Delta y_{CH_4}$  i.e.,  $y_{CH_4}^{PRN} - y_{CH_4}^{CRN}$  (c) product (CO) mole fractions obtained when using the comprehensive reaction network (CRN) in red vs the partial reaction network (PRN) in blue, and (d)  $\Delta y_{CO}$  i.e.,  $y_{CO}^{PRN} - y_{CO}^{CRN}$ , observed over Ni(1 1 1). (For interpretation of the references to colour in this figure legend, the reader is referred to the web version of this article.)

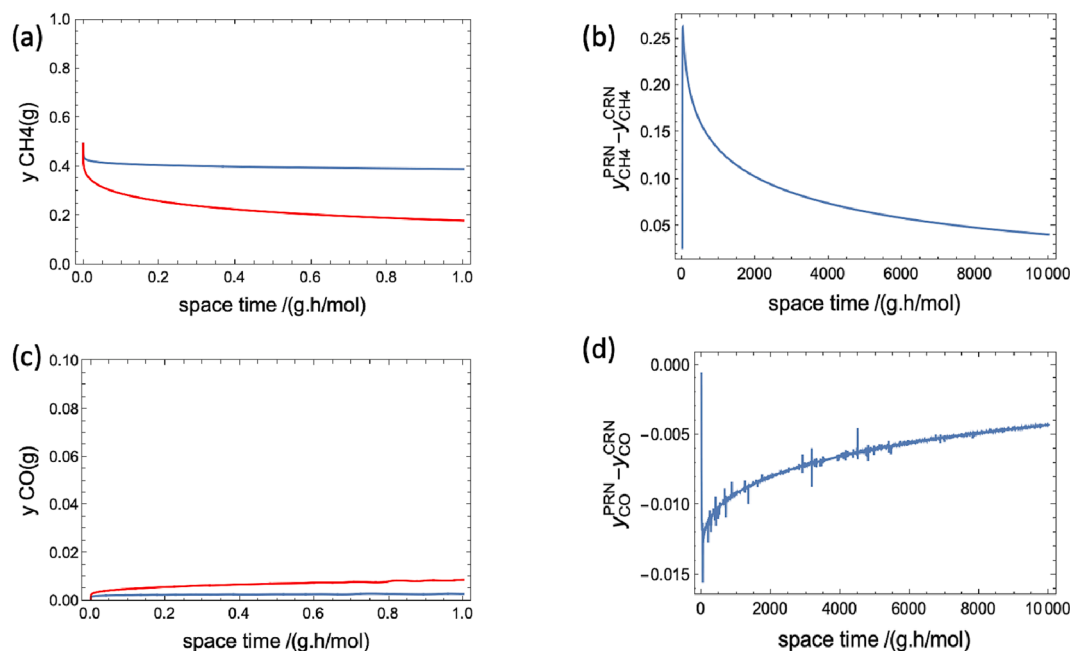


**Fig. 7.** Model predictions of (a) reactant (CH<sub>4</sub>) mole fraction when using the comprehensive reaction network (CRN) (red) vs the partial reaction network (PRN) (blue), (b)  $\Delta y_{CH_4}$  i.e.,  $y_{CH_4}^{PRN} - y_{CH_4}^{CRN}$  (c) product (CO) mole fractions obtained when using the comprehensive reaction network (CRN) in red vs the partial reaction network (PRN) in blue, and (d)  $\Delta y_{CO}$  i.e.,  $y_{CO}^{PRN} - y_{CO}^{CRN}$ , observed over B-doped Ni or NiB(1 1 1). (For interpretation of the references to colour in this figure legend, the reader is referred to the web version of this article.)

a consistent trend is observed between PRN-1 vs CRN model predictions for all three Ni-based systems. The reactant mole fractions for both models are such that  $y_{CH_4}^{PRN} \geq y_{CH_4}^{CRN}$ , whereas the product mole fractions are such that  $y_{CO}^{PRN} \geq y_{CO}^{CRN}$ . This observation is consistent for the entire range of reactor space-times, even as the reaction reaches equilibrium, see Figs. 6-8. However, to confirm this generalization for PRN vs CRN model outcomes, the same observation should uphold for PRNs with

different pathway combinations and energetics. Congestion and accumulation of mass-flow in a PRN could easily reverse the observed trends. Therefore, to understand how PRNs prediction varies depending on pathways, i.e. unmuted reaction steps, separate investigations are performed to understand the effects of congestion and accumulation.

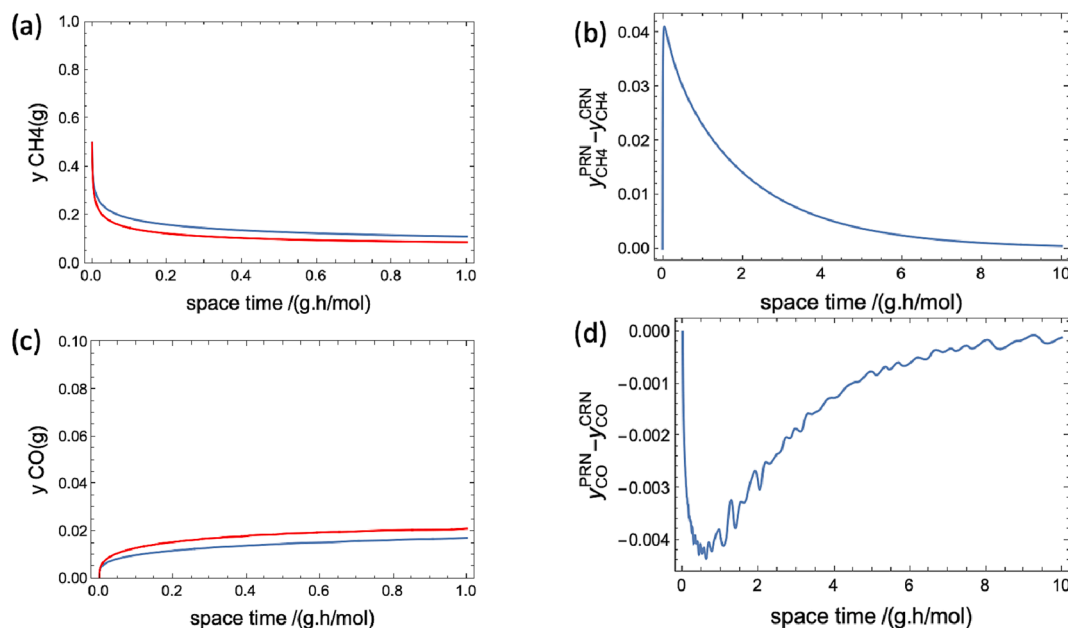


**Fig. 8.** Model predictions of (a) reactant (CH<sub>4</sub>) mole fraction when using the comprehensive reaction network (CRN) (red) vs the partial reaction network (PRN) (blue), (b)  $\Delta y_{CH_4}$  i.e.,  $y_{CH_4}^{PRN} - y_{CH_4}^{CRN}$ , (c) product (CO) mole fractions obtained when using the comprehensive reaction network (CRN) in red vs the partial reaction network (PRN) in blue, and (d)  $\Delta y_{CO}$  i.e.,  $y_{CO}^{PRN} - y_{CO}^{CRN}$ , observed over Ni-based Hypothetical catalyst (NiHC). (For interpretation of the references to colour in this figure legend, the reader is referred to the web version of this article.)

### 3.2. Mass-flow representation of catalyst performance

A reaction mechanism includes elementary steps corresponding to: (i) reactant dissociation, (ii) intermediate association to form products, and (iii) side reactions. The catalytic activity is, therefore, obtained as a function of energy barriers corresponding to these steps and catalyst optimization is always concerned with reducing energy barriers of relevant reaction steps. For example, the rate-determining step is often used as a descriptor for screening catalysts [40]. Similarly, catalyst stability is predicted in terms of intermediate binding energies.

However, ensuring reasonable values for both energy barriers and binding energies does not necessarily result in a high-performing catalyst. A simple descriptor-based prediction of catalyst performance can fall short in many complex reaction systems like DRM. Complex reaction systems have multiple interlinked pathways for products formation. Moreover, the energy barriers and binding energies of a catalyst are always related and cannot be optimized independently. This has been observed in the case of Ni(111) and NiB(111) catalysts when comparing their catalyst performance for DRM. It can be seen from Table S4 that the energy barriers for reactant dissociation are lower for NiB(1 1 1). However, the activity of Ni(1 1 1) is higher. In the case of NiB(1 1 1), even if the reactant dissociation and CH<sub>2</sub> oxidation barriers are lower than Ni(1 1 1), the surface coverages of the reactant species fall short in the rate equations (Equation (7)) due to mass-flow distribution among competing pathways (a reference to Table 1 for further comparison). Hence, catalytic performance is only confirmed through a thorough analysis using comprehensive reaction models.

Given the intricate complexity and interdependency of reaction networks, it can be seen as a representation of mass-flow from reactants to products. This representation simplifies the previously interdependent reaction energetics into a flow system with accumulation and congestion depending on the energetics and topology of the reaction network. Therefore, instead of focusing on specific descriptors, catalyst performance will be enhanced by limiting congestion and accumulation of mass-flow from reactants to products.

Before progressing with the mass flow analysis, it is important to understand mass-flow accumulation and congestion when looking at a

reaction network. The following section briefly describes the two phenomena for the scope of this study.

### 3.3. Accumulation and congestion in reaction networks

Accumulation occurs when the intermediate formation rate is greater than the consumption in a given reaction network, i.e. mass-flow from reactants piles up as intermediate instead of product formation. For example, C\* formation over Ni during DRM. The accumulation of an intermediate depends on the energy difference between its binding energy and neighbouring transition state barriers. It also depends on the extent of mass flow and connectivity. The intermediates in close proximity to the reactant are likely to accumulate first, leading to a lower mass flow down the network, thereby reducing the chances of further accumulation. This sort of dependence of accumulation on network topology has been tested for the case of an absolute random catalyst that favours all reaction steps equally. The extent of accumulation of an intermediate w.r.t. other intermediates can be compared based on fractional surface coverages (see Table 1 in section 3.4). Please refer to Table S4 and Section 5 of SI for more details.

Just as accumulation results from mass-flow being piled up as intermediates, congestion occurs when the full capacity of a pathway (set of reaction steps) is not realised due to multiple interlinked competing pathways. For example, DRM rate in Figure S4 is lower for NiB(1 1 1) compared to Ni(1 1 1) due to multiple competing pathways in NiB(1 1 1), even though NiB's reactant dissociation barriers are lower, see Table S4.

Congestion as a network phenomenon, arising due to network topology, has been investigated for varying problems across different fields of knowledge, such as traffic planning, pipeline flow and electrical circuits. Although unlike the roadways and other flow systems, the extent of congestion in a reaction network depends on both topology, kinetics and mass accumulation at nodes (intermediates). For example, the topology of the DRM network, Fig. 3, resembles regular network topology in urban traffic [41] which is inherently prone to congestion. However, reaction kinetics may place a significant weight on a particular pathway, as illustrated in Fig. 4a, thus preventing congestion. Similar observation has been reported [34] for a chemical system

**Table 1**

Intermediate coverages observed over different catalyst surfaces at 973 K, 10 bar and a reactor space time of  $1 \text{ g}\cdot\text{h}\cdot\text{mol}^{-1}$ . The coverages are also reported for an absolute random catalyst (ARC) when varying the reaction network.

Species	Ni (1 1 1)	NiB (1 1 1)	NiHC	ARC CRN	PRN	PRN-2
CH <sub>3</sub> *	$1.05 \times 10^{-7}$	$1.22 \times 10^{-5}$	$3.84 \times 10^{-8}$	$1.82 \times 10^{-1}$	0.2154	0.1950
CH <sub>2</sub> *	$2.45 \times 10^{-7}$	$5.76 \times 10^{-8}$	$1.21 \times 10^{-7}$	$6.93 \times 10^{-2}$	0.0895	0.0908
CH*	$2.32 \times 10^{-5}$	$1.27 \times 10^{-7}$	$1.44 \times 10^{-5}$	$2.09 \times 10^{-2}$	0.0238	0.0264
C*	$6.00 \times 10^{-7}$	$1.58 \times 10^{-9}$	$9.15 \times 10^{-8}$	$1.45 \times 10^{-2}$	0.0055	0.0066
CO <sub>2</sub> *	$2.68 \times 10^{-7}$	$3.95 \times 10^{-5}$	$2.65 \times 10^{-7}$	$1.00 \times 10^{-1}$	0.2397	0.1006
CO*	$8.10 \times 10^{-1}$	$7.70 \times 10^{-1}$	$8.75 \times 10^{-1}$	$5.99 \times 10^{-2}$	0.0665	0.0595
COOH*	$1.67 \times 10^{-9}$	$1.36 \times 10^{-7}$	$5.16 \times 10^{-10}$	$6.99 \times 10^{-2}$	–	0.0714
HCOO*	$6.70 \times 10^{-7}$	$3.06 \times 10^{-3}$	$1.00 \times 10^{-5}$	$7.03 \times 10^{-2}$	–	0.0923
HCO*	$2.88 \times 10^{-8}$	$1.10 \times 10^{-7}$	$1.77 \times 10^{-8}$	$4.04 \times 10^{-2}$	0.0245	0.0143
HCOOH*	$9.77 \times 10^{-11}$	$4.35 \times 10^{-10}$	$7.09 \times 10^{-12}$	$5.30 \times 10^{-2}$	–	0.0725
CH <sub>3</sub> OH*	$7.77 \times 10^{-11}$	$2.33 \times 10^{-10}$	$4.81 \times 10^{-12}$	$2.48 \times 10^{-2}$	–	0.0195
CH <sub>2</sub> OH*	$1.70 \times 10^{-13}$	$1.05 \times 10^{-10}$	$5.09 \times 10^{-14}$	$1.10 \times 10^{-2}$	–	0.0035
CHOH*	$8.49 \times 10^{-12}$	$6.20 \times 10^{-11}$	$5.96 \times 10^{-12}$	$7.26 \times 10^{-3}$	–	0.0018
COH*	$1.80 \times 10^{-7}$	$5.67 \times 10^{-11}$	$3.67 \times 10^{-8}$	$1.13 \times 10^{-2}$	–	0.0112
CH <sub>3</sub> O*	$5.28 \times 10^{-9}$	$2.86 \times 10^{-8}$	$2.05 \times 10^{-10}$	$5.57 \times 10^{-2}$	–	0.0490
CH <sub>2</sub> O*	$7.31 \times 10^{-11}$	$1.79 \times 10^{-9}$	$9.93 \times 10^{-11}$	$2.71 \times 10^{-2}$	–	0.0120
H <sub>2</sub> O*	$1.65 \times 10^{-5}$	$7.10 \times 10^{-4}$	$5.44 \times 10^{-5}$	$6.13 \times 10^{-3}$	0.0127	0.0056
O*	$1.04 \times 10^{-2}$	$2.06 \times 10^{-3}$	$9.55 \times 10^{-4}$	$4.18 \times 10^{-2}$	0.1068	0.0640
H*	$2.77 \times 10^{-2}$	$8.29 \times 10^{-3}$	$1.21 \times 10^{-2}$	$6.10 \times 10^{-2}$	0.1041	0.0322
OH*	$6.87 \times 10^{-4}$	$7.51 \times 10^{-3}$	$1.05 \times 10^{-3}$	$2.25 \times 10^{-2}$	0.0436	0.0191
Free Site (*)	$1.26 \times 10^{-1}$	$1.25 \times 10^{-1}$	$9.53 \times 10^{-2}$	$5.13 \times 10^{-2}$	0.0680	0.0528

inspired by Braess' paradox [42]. Congestion in the network was only observed for a certain range of rate constants and reaction times wherein predicted product mole fraction was overestimated when a certain pathway was eliminated by muting a reaction step, i.e. their PRN was overestimating the product mole fraction.

Despite such observations, congestion [34,43] is not found in Figs. 6–8. This is because these Ni-based catalysts favour specific pathways over the others that correspond to an apparent reaction network (network including kinetically relevant pathways), see Table S3 in SI for further details. This apparent reaction network is the same as Fig. 4a and is a subset of the CRN.

However, a CRN is prone to congestion if all reaction steps are equally favoured, i.e. energetics are corresponding to an absolute random catalyst (ARC) in Fig. 5. For more details regarding the ARC please refer to Section 2.2. Model results predicted over the ARC are discussed in Section 3.4.

### 3.4. Congestion in the comprehensive reaction network

The earlier study on reaction network congestion [34] conducted an investigation wherein the partial network included all intermediates from the comprehensive network. This neutralized the effect of intermediate' accumulation over the final model outcomes, i.e. reactant

conversions and product formation. Therefore, an additional partial reaction network (PRN-2) is constructed to perform a similar analysis by including all DRM intermediates (Fig. 3). Three independent pathways for CO formation from CH<sub>4</sub> are also included. Please refer to Section 2.1 for more details regarding the reaction steps. The reactant' and the product's mole fractions are then predicted using models based on PRN-1, PRN-2 and CRN. The differences in predictions between the two partial network models and the CRN/ARC model are shown in Fig. 9.

From Fig. 9 one can observe that near equilibrium, the PRN-2/ARC model predicts network congestion similar to the previous study [34], i.e. the reactant's mole fractions are lower than those predicted by the CRN model ( $y_{\text{CH}_4}^{\text{PRN}} < y_{\text{CH}_4}^{\text{CRN}}$ ) and the product' mole fractions are higher than those predicted by the CRN model ( $y_{\text{CO}}^{\text{PRN}} > y_{\text{CO}}^{\text{CRN}}$ ). However, the PRN-1/ARC model overestimates both the reactant' and the product' mole fractions at equilibrium. The overestimation of CO mole fraction by PRN-1/ARC model is even higher than the values obtained with the PRN-2/ARC model.

This difference in equilibrium mole fractions is caused due to missing intermediate / reaction steps in the network (please refer to Section 6 of SI). However, whether the estimated mole fraction is higher or lower than CRN models, depends on both congestion and accumulation. The CRN/ARC is inherently prone to congestion and accumulation. This congestion is, however, not observed in PRN-1/ARC due to the absence of other pathways. The PRN-1/ARC model also lacks dynamic mass accumulation in the form of intermediate concentration/coverage.

In the case of reactant mole fractions, the absence of congestion and accumulation have contradictory effects. The absence of accumulation lowers the reactant conversion (higher reactant mole fraction) since the capacity of the network is reduced, whereas the absence of congestion allows more mass flow through the pathways, i.e. higher reaction rates, higher reactant conversions and lower reactant mole fractions. Contrarily, in the case of reactant mole fractions, the absence of congestion and accumulation have the same effects. The absence of accumulation causes more mass-flow out of the network as product (higher product mole fraction) since the capacity of the network is reduced, whereas the absence of congestion allows higher reaction rates and more product formation. Therefore, the difference in reactant and product mole fraction prediction between PRN-1/ARC and CRN/ARC is a combined result of congestion and accumulation phenomena.

In the case of PRN-2/ARC, all CRN intermediates are included in the model and each reaction step is equally favoured. Therefore, the extent of accumulation in PRN-2/ARC is very similar to CRN/ARC and the difference the in reactant and product mole fraction prediction between PRN-2/ARC and CRN/ARC depends on whether there is congestion in the PRN-2/ARC model at a given reactor space-time. This means,  $y_{\text{CH}_4}^{\text{PRN-2}} - y_{\text{CH}_4}^{\text{CRN}}$  will be negative and  $y_{\text{CO}}^{\text{PRN-2}} - y_{\text{CO}}^{\text{CRN}}$  will be positive (as shown in Fig. 9c, d) if congestion is absent in PRN-2/ARC and accumulation is comparable to CRN/ARC.

Another observation that is made from this analysis is the surface coverages listed in Table 1 for PRN-2. The coverages suggest that when all reaction steps are favoured equally (ARC), intermediates closer to reactants (least # reaction steps away) have higher fractional coverages compared to the others, e.g. CO<sub>2</sub>\*, CH<sub>3</sub>\*. Therefore, when energetics supports the accumulation of multiple intermediates equally, the likelihood for accumulation of a particular intermediate will depend on its proximity from the reactants, i.e. minimum # reaction steps from reactant.

### 3.5. Reactant (CH<sub>4</sub>) mole fraction predicted by PRN models for catalyst screening

From the analysis based on ARC, it is concluded the absence of accumulation and congestion in PRN (PRN-1, PRN-2) increases the overall difference  $y_{\text{CO}}^{\text{PRN}} - y_{\text{CO}}^{\text{CRN}}$ , but the effects negate each other when

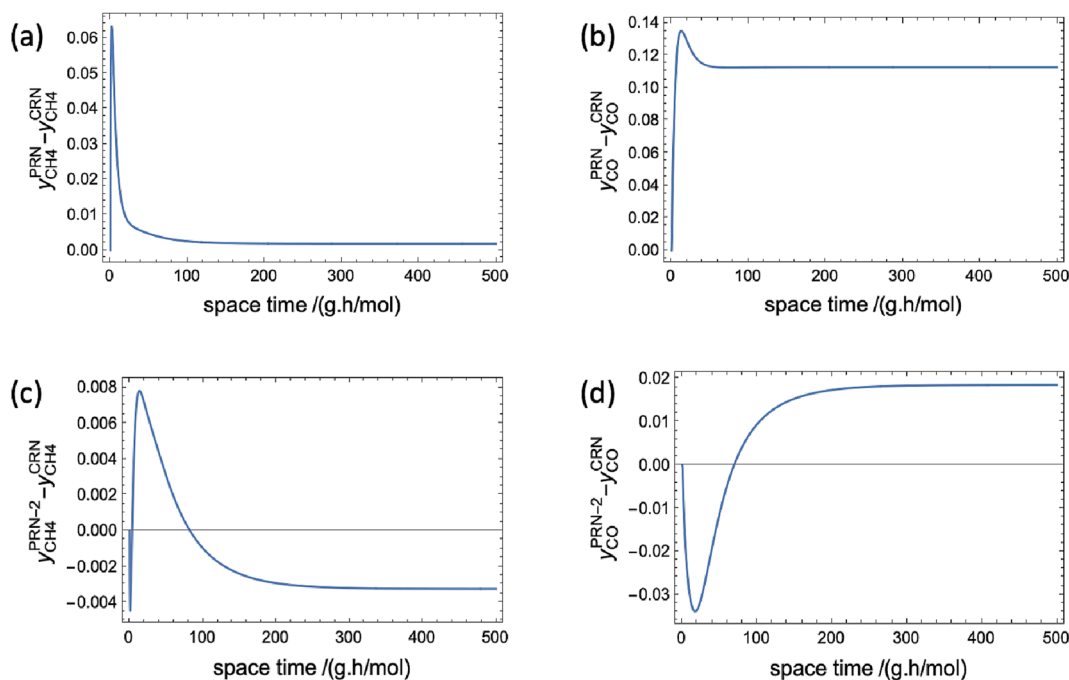


**Fig. 9.** A comparison of model predictions of (a)  $y_{CH_4}^{PRN} - y_{CH_4}^{CRN}$ , (b)  $y_{CO}^{PRN} - y_{CO}^{CRN}$ , (c)  $y_{CH_4}^{PRN-2} - y_{CH_4}^{CRN}$ , (d)  $y_{CO}^{PRN-2} - y_{CO}^{CRN}$ , obtained over an absolute random catalyst (ARC). Where PRN, PRN-2 correspond to the partial reaction networks in Fig. 2b and 3, and CRN corresponds to the comprehensive reaction network in Fig. 2a.

computing the difference  $y_{CH_4}^{PRN} - y_{CH_4}^{CRN}$ . Making  $y_{CH_4}^{PRN} - y_{CH_4}^{CRN}$  a more robust metric for comparing catalyst performance. Furthermore, from Fig. 6b, 7b, 8b and 9a, it is observed that the difference in reactant mole fraction ( $y_{CH_4}^{PRN} - y_{CH_4}^{CRN}$ ) predicted by the PRN-1 and CRN models is positive throughout the reactor space-time, regardless of the catalyst energetics (real catalysts, NiHC, ARC).

However, the case of product mole fraction is not so generalizable.  $y_{CO}^{PRN} - y_{CO}^{CRN}$  is positive over ARC (Fig. 9b) whereas,  $y_{CO}^{PRN} - y_{CO}^{CRN}$  is negative over Ni-based catalysts (Fig. 6d, Fig. 7d and Fig. 8d). This is because ARC favours all reaction steps equally and the CRN/ARC model suffers from mass-flow accumulation and congestion, therefore, PRN-1 leads to more product formation. Contrarily, Ni-based systems favour only particular pathways at a time, see Table S3. Thus, unlike the CRN/ARC models, the CRN/real catalyst model is not prone to congestion. Additionally, the most abundant intermediate over Ni-based catalyst (computed using the CRN model) is surface CO or CO\* that corresponds to < 70% fraction coverage. This prevents carbon mass accumulation as intermediates that are not part of the PRN-1. The CRN/real catalyst model also includes additional independent pathways. Like the formation of oxidizing agents (O\*, OH\*) from CO<sub>2</sub> via H-induced CO<sub>2</sub> dissociation (R7-13, in Table S2) and CO formation via COH\* dehydrogenation. These pathways have a small contribution towards CO\* formations which is insignificant compared to the dominant pathway. However, their absence in the PRN-1/real catalyst model leads to a negative  $y_{CO}^{PRN} - y_{CO}^{CRN}$  in Fig. 6d, Fig. 7d and Fig. 8d.

The generalizability of  $y_{CH_4}^{PRN} - y_{CH_4}^{CRN}$  for PRN-1 makes this difference a more robust and reliable metric for comparing catalyst performance for models that only include the dominant pathway. That is, a PRN that contains reaction steps and relevant intermediates corresponding to the dominant pathways and side reactions will overestimate the reactant mole fraction. This inequality is reported in Equations 9–11.

$$\Delta y_R = y_R^{PRN} - y_R^{CRN} \geq 0 \quad (9)$$

$$\Delta x_R = x_R^{PRN} - x_R^{CRN} \leq 0 \quad (10)$$

$$x_R = 1 - \frac{y_R}{(y_R)_0} \quad (11)$$

where,  $R$  corresponds to the reactants  $(y_R)_0$  and is the initial reactant mole fraction at reactor input. For DRM reaction system,  $R = CH_4$ .

Knowing the lowest achievable reactant' conversion on a specific catalyst could allow activity comparisons using PRNs. This is important since computing energetics of an entire CRN is very expensive. Therefore, further analysis is done to test the consistency of this observation (Equation (9)) and to further identify regions based on catalysts energetics where this observation is true. Hundreds of NiHC (please refer to Section 2.2 for details) with varying energetics were created for this analysis. Results are reported in Section 3.6.

### 3.6. Partial reaction networks vs catalyst energetics

Reactant conversions as predicted by the PRN-1 and the CRN-based models were computed for 200 NiHCs whose energetics (intermediate/transition state energies,  $\Delta E_{IS/TS}$ ) differ within  $\pm 50$  kJ mol<sup>-1</sup> from that observed over Ni(111). A histogram and box plot charts (see Figures S6 and S7 in SI) illustrate the distribution of this energy difference from Ni(111) for C ( $\Delta E_C$ ) and O ( $\Delta E_O$ ) and scaling relation slopes ( $\gamma(x), \alpha$ ) corresponding to the remaining intermediates. Please refer to Section 2.2 for more details on constructing NiHCs.

Fig. 10a shows the differences in reactant mole fractions  $\Delta y_{CH_4}$  between the PRN and the CRN-based model predictions for the 200 different scenarios. The inequality mentioned in Equations 9–11 is satisfied for all the 200 NiHCs when the  $\Delta E$  bounds are  $\pm 50$  kJ mol<sup>-1</sup>. The energy distribution in Figure S6 suggests that due to the added constraints in Equations 1–5, the majority of NiHCs lie within a  $\Delta E_C$  and  $\Delta E_O$  value of  $\pm 20$  kJ mol<sup>-1</sup>, which is not a very significant difference. Therefore, a similar analysis was performed with the bounds on  $\Delta E_{IS/TS}$  increased to  $\pm 100$  kJ mol<sup>-1</sup>.

From Fig. 10b one can see that a handful of instances do not satisfy the inequality in Equations 9–10. Upon closer examination, it is found that the coverages corresponding to intermediates not included in the PRN-1, like HCOO\*, become relevant at a given space-time. For

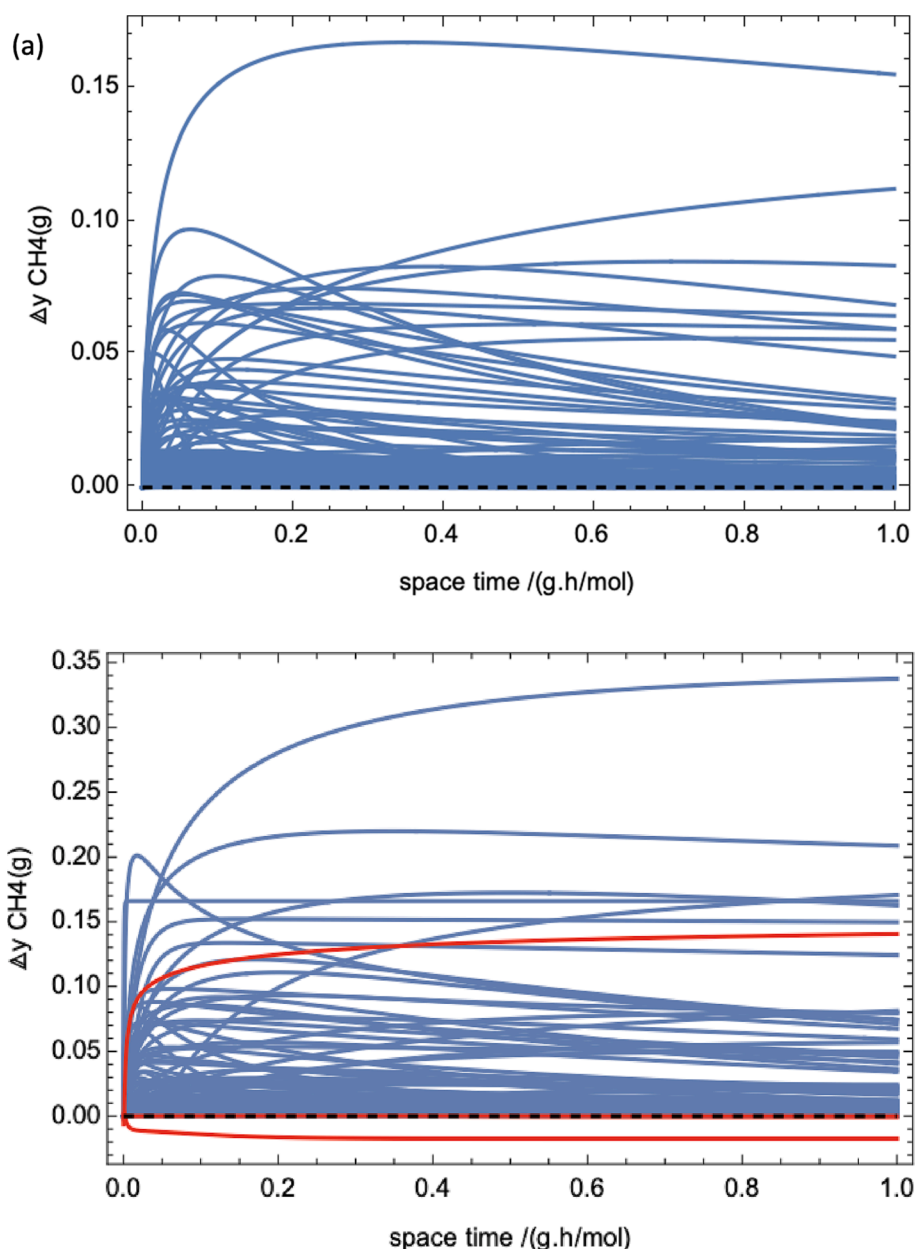


**Fig. 10.** Difference between PRN vs CRN-based model predictions of reactant mole fraction ( $\Delta y_{CH_4} = y_{CH_4}^{PRN} - y_{CH_4}^{CRN}$ ) obtained over 200 Ni-based hypothetical catalysts when  $\Delta E$  bounds are within  $\pm 50$  kJ mol<sup>-1</sup> (a) and  $\pm 100$  kJ mol<sup>-1</sup>. The hypothetical catalysts for which  $\Delta y_{CH_4} < 0$  at any reaction space-time from 0 to 1 g•h•mol<sup>-1</sup>, are shown in red. (For interpretation of the references to colour in this figure legend, the reader is referred to the web version of this article.)

example, NiHC #70 does not satisfy the inequality in Equations 9–10 and HCOO\* fractional coverage over this catalyst is found to be 0.043 at 1 g•h•mol<sup>-1</sup> obtained using the CRN-based model. It is the 2nd most abundant species and its fractional coverage over the hypothetical catalyst is much higher than the value of  $6.70 \times 10^{-7}$  observed over Ni (1 1 1) at 1 g•h•mol<sup>-1</sup>. Higher fractional coverage suggests that HCOO\* intermediate consumes oxidizing agents which would otherwise react with CH<sub>x</sub> species, thus limiting reactant conversions and product formation. Additionally, a significant coverage suggests catalyst poisoning because the free sites are occupied by a stable intermediate and cannot be used for the main reaction. Therefore, excluding HCOO\* intermediate from the PRN-1 leads to higher reactant conversions and product formation. In other words, the current PRN does not contain relevant side reactions (HCOO\* formation), which seems to be a necessary requirement to satisfy inequalities in Equations (9),(10).

A new PRN, which includes HCOO\* formation, is constructed. The

dominant reaction step for HCOO\* from CO<sub>2</sub> is found to be via CO<sub>2</sub>(g) → CO<sub>2</sub> → HCOO\*, whereas for CH<sub>4</sub> it is CH<sub>4</sub>(g) → CH<sub>3</sub>\* → CH<sub>2</sub>\* → CH\* → CHO\* → CO\* → CO<sub>2</sub>\*+\* → CO<sub>2</sub>\* → HCOO\*. Since the only reaction step present in the above-listed pathways but missing in the current PRN is CO<sub>2</sub>\* → HCOO\* (R7 of DRM in Table S2), therefore, only this reaction step is included in the updated PRN.

From Fig. 11 it is seen that once HCOO\* formation is included in the PRN, the inequality in Equations 9–10 is satisfied. A similar strategy is implemented for the remaining hypothetical catalysts where inequalities (9–10) are not satisfied; details are reported in Section 8 of the SI. It is found that HCOO\* is a relevant intermediate for all of these hypothetical catalysts, see Figure S8-S11. However, there could be more than one competing pathway for HCOO\* formation from CH<sub>4</sub> and CO<sub>2</sub>. Sometimes these pathways also include the formation of other intermediates (e.g. COOH\*, COH\*) that eventually react to form HCOO\*, see Figure S8.

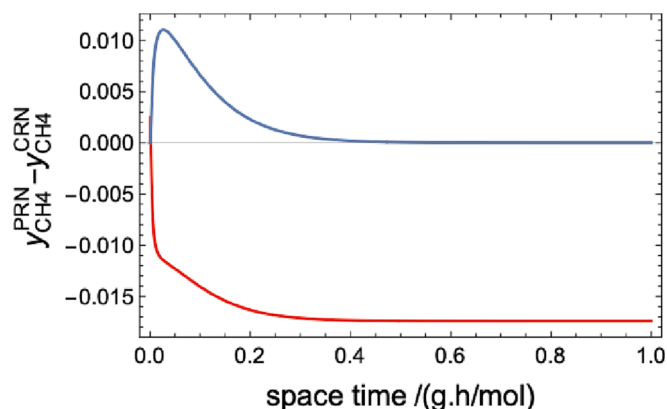


**Fig. 11.** Difference between PRN vs CRN based model predictions of reactant mole fraction ( $\Delta y_{CH_4} = y_{CH_4}^{PRN} - y_{CH_4}^{CRN}$ ) obtained over NiHC#70 ( $\Delta E$  bounds are within  $\pm 100 \text{ kJ mol}^{-1}$ ), when  $\text{HCOO}^*$  formation via  $\text{CO}_2^*$  hydrogenation is not included in the PRN (red), and when it is included in the PRN (blue). (For interpretation of the references to colour in this figure legend, the reader is referred to the web version of this article.)

Even though including all reaction steps / intermediates corresponding to dominant pathways for  $\text{HCOO}^*$  in the existing PRN leads to reaction conversions that satisfy inequalities (9–10), the same can be achieved by including a subset of these reaction steps/intermediates (see Figures S8 and S11). This is particularly important since including a subset of reaction steps/intermediates is computationally less expensive. Therefore, the stepwise workflow reported in Fig. 5 should be used to construct a transferable PRN that satisfies inequalities 9–10, for a given  $\Delta E$  by identifying additional reaction steps/intermediates that need to be included in a PRN based on an initial catalyst.

#### 4. Transferability of partial reaction networks and limitations

Once the final PRN is constructed, catalyst activity prediction in terms of minimum reactant conversion can be performed within the energy bounds designated for the hypothetical catalyst analysis without experimental validation. Possible catalyst poisoning via intermediate formation can also be predicted using the hypothetical catalyst analysis. The PRN obtained via these design rules (see Fig. 5), can be implemented to different compositional variations of Ni and even other metallic systems like Ru (see Fig. 12), where  $\Delta E_{C/O}$  w.r.t. to Ni(111) are within the energy bounds explored for hypothetical catalysts satisfying minimum reactant conversion of PRN.

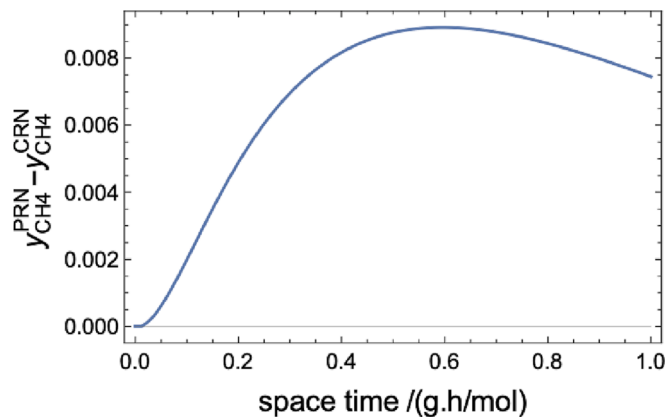


**Fig. 12.** A difference in PRN vs CRN based model predictions of reactant mole fraction ( $\Delta y_{CH_4} = y_{CH_4}^{PRN} - y_{CH_4}^{CRN}$ ) obtained over Ru (001), where the PRN was constructed based on the workflow using Ni(111) as the initial catalyst guess.

The same generalization cannot be made for product yield prediction using PRNs since product yield is very sensitive to the reaction network (a reference to Section 3.5). Therefore, yield and selectivity must be predicted using models based on the experimentally verified comprehensive reaction network.

Apart from product yield and sensitivity prediction, there is an additional limitation to using the PRN-based models - model stiffness, i.e. when the solution curve displays significant variation due to numerical instability of the mass balance equations. A further investigation based on the  $\text{CO}_2$  methanation reaction system highlights this issue and its implications on using the PRN-based models. The  $\text{CO}_2$  methanation reaction model has been observed to demonstrate a stiff behaviour due to the larger number of reaction steps and intermediate variables when compared against DRM. This inherent model stiffness makes it difficult to progress with hypothetical catalyst analysis. Figure S13 demonstrates this problem for hypothetical catalyst analysis performed using a PRN (Figure S12 in Section 9 of SI) that works for Ni(111). The  $\Delta y_R$  values, where  $R = \text{CO}_2$ , are found to oscillate around  $y = 0$ , unless the PRN is the same as the CRN, i.e. all reaction steps are included in the network. This limits the applicability of PRN design rules. Figure S13 suggests that these fluctuations can be as high as  $10^{-3}$ , depending on the magnitude of its corresponding reaction fractional conversion.

For such model systems it is very important to determine whether the failure in design rules is due to model stiffness. Both intermediate accumulation and model stiffness can lead to negative  $\Delta y_R$ , however, numerical stability of system can be analysed via inflection points in kinetic plots. Once stiffness and stability of the model predictions are confirmed for the required reactor space-time, design rules in Fig. 5 can be applied to construct a partial reaction network.

#### 5. Conclusions

Partial reaction networks (PRNs) are often used in theoretical investigations involving catalytic performance comparison due to lower cost of investigation, compared to a comprehensive reaction network (CRN). However, the transferability of a PRN developed over an initial catalyst guess, like Ni(111), cannot be guaranteed for even slight modifications, like NiB(111), unless validated experimentally over both surfaces. Therefore, in this study, we develop guidelines for constructing PRNs using dominant pathways for comparing catalyst performances over different material compositions, in the absence of experimental/DFT data.

We start by implementing a mass-flow analogy to represent catalyst performances in terms of congestion and accumulation. It is found that congestion and accumulation in a reaction network are dependent on its topology and kinetics, thus the overall model predictions i.e., reactant conversions, and product concentration, are different for a CRN and a PRN. Even so, some consistencies are observed for the reactant conversion predictions. Compared to a CRN model, a PRN model, including dominant pathways, side reaction and relevant species, is found to always under-estimates the reactant conversion.

Therefore, we investigate this hypothesis for a set of 200 Ni-based hypothetical catalysts that were created by varying DFT energies of intermediates and transition states over Ni(111) by up to  $\pm 100 \text{ kJ mol}^{-1}$ . Based on this investigation, we developed a workflow for constructing transferable PRNs (within certain surface energy bounds) without experimental/DFT data. The PRNs developed via this workflow are simple, yet representative enough to screen a list of catalysts based on minimum reactant conversion for further expensive investigation.

Aside from broadening the applications of micro-kinetic models in catalyst investigation, the techniques presented in this study can also be used for adding complexity to reaction networks in an efficient stepwise manner. The models based on the workflow presented in this study can also assist and complement expensive investigations like designing catalyst compositions for improved performance. It further complements experimental investigations by screening materials for validation.

## Author contributions

Shambhawi designed the study, developed methods, performed analysis, wrote draft manuscript and worked on revisions. JMW advised on network theory, corrected manuscript. AAL developed the project's concept, supervised overall project, corrected manuscript.

## Declaration of Competing Interest

The authors declare that they have no known competing financial interests or personal relationships that could have appeared to influence the work reported in this paper.

## Data availability

No data was used for the research described in the article.

## Acknowledgements

Shambhawi acknowledges the research scholarship funding from Science and Engineering Research Board, India and Cambridge Trust. This work was in part supported by National Research Foundation (NRF), Prime Minister's Office, Singapore under its Campus for Research Excellence and Technological Enterprise (CREATE) program as a part of the Cambridge Centre for Advanced Research and Education in Singapore Ltd (CARES), and Engineering and Physical Sciences Research Council via project EP/S024220/1 EPSRC Centre for Doctoral Training in Automated Chemical Synthesis Enabled by Digital Molecular Technologies.

## Appendix A. Supplementary data

Supplementary data to this article can be found online at <https://doi.org/10.1016/j.cej.2023.143212>.

## References

- M. Boudart, From the century of the rate equation to the century of the rate constants: a revolution in catalytic kinetics and assisted catalyst design, *Catal. Lett.* 65 (1) (2000) 1–3.
- Marin, G.B., G.S. Yablonsky, and D. Constales, *Kinetics of Chemical Reactions. Decoding Complexity*. 2nd ed. 2019: Wiley-VCH. 442 pp.
- A.H. Motagamwala, J.A. Dumesic, Microkinetic Modeling: A Tool for Rational Catalyst Design, *Chem. Rev.* 121 (2) (2021) 1049–1076.
- C.F. Goldsmith, R.H. West, Automatic Generation of Microkinetic Mechanisms for Heterogeneous Catalysis, *J. Phys. Chem. C* 121 (18) (2017) 9970–9981.
- S. Maeda, T. Taketsugu, K. Morokuma, Exploring transition state structures for intramolecular pathways by the artificial force induced reaction method, *J Comput Chem* 35 (2) (2014) 166–173.
- P.M. Zimmerman, Automated discovery of chemically reasonable elementary reaction steps, *J. Comput. Chem.* 34 (16) (2013) 1385–1392.
- Q. Zhao, B.M. Savoie, Simultaneously improving reaction coverage and computational cost in automated reaction prediction tasks, *Nature Computational Science* 1 (7) (2021) 479–490.
- C.W. Gao, J.W. Allen, W.H. Green, R.H. West, Reaction Mechanism Generator: Automatic construction of chemical kinetic mechanisms, *Comput. Phys. Commun.* 203 (2016) 212–225.
- M. Liu, A. Grinberg Dana, M.S. Johnson, M.J. Goldman, A. Jocher, A.M. Payne, C. A. Grambow, K. Han, N.W. Yee, E.J. Mazeau, K. Blondal, R.H. West, C. F. Goldsmith, W.H. Green, Reaction Mechanism Generator v3.0: Advances in Automatic Mechanism Generation, *J. Chem. Inf. Model.* 61 (6) (2021) 2686–2696.
- K. Delgado, L. Maier, S. Tischer, A. Zellner, H. Stotz, O. Deutschmann, Surface Reaction Kinetics of Steam- and CO<sub>2</sub>-Reforming as Well as Oxidation of Methane over Nickel-Based Catalysts. 5 (2) (2015) 871–904.
- M. Jarafz, J.E. Rubio, L. Enriquez, R. Pinacho, J.L. López-Pérez, A. Lesarri, An Efficient Microkinetic Modeling Protocol: Start with Only the Dominant Mechanisms, Adjust All Parameters, and Build the Complete Model Incrementally, *ACS Catal.* 9 (6) (2019) 4804–4809.
- L.C. Grabow, M. Mavrikakis, Mechanism of Methanol Synthesis on Cu through CO<sub>2</sub> and CO Hydrogenation, *ACS Catal.* 1 (4) (2011) 365–384.
- M. Stamatakis, D.G. Vlachos, A graph-theoretical kinetic Monte Carlo framework for on-lattice chemical kinetics, *J. Chem. Phys.* 134 (21) (2011) 214115.
- I. Fishtik, R. Datta, A UBI-QEP microkinetic model for the water–gas shift reaction on Cu(111), *Surf. Sci.* 512 (3) (2002) 229–254.
- O. Mohan, Q.T. Trinh, A. Banerjee, S.H. Mushrif, Predicting CO<sub>2</sub> adsorption and reactivity on transition metal surfaces using popular density functional theory methods, *Mol. Simul.* 45 (14–15) (2019) 1163–1172.
- Y. Lu, et al., Quantifying the error propagation in microkinetic modeling of catalytic reactions with model-predicted binding energies, *Mol. Catal.* 530 (2022), 112575.
- A.J. Medford, J. Wellendorff, A. Vojvodic, F. Studt, F. Abild-Pedersen, K. W. Jacobsen, T. Bligaard, J.K. Nørskov, Assessing the reliability of calculated catalytic ammonia synthesis rates, *Science* 345 (6193) (2014) 197–200.
- M. Andersen, C.P. Plaisance, K. Reuter, Assessment of mean-field microkinetic models for CO methanation on stepped metal surfaces using accelerated kinetic Monte Carlo, *J. Chem. Phys.* 147 (15) (2017) 152705.
- A.B. Mhadeshwar, D.G. Vlachos, Is the water–gas shift reaction on Pt simple?: Computer-aided microkinetic model reduction, lumped rate expression, and rate-determining step, *Catal. Today* 105 (1) (2005) 162–172.
- T.P. de Carvalho, R.C. Catapan, A.A.M. Oliveira, D.G. Vlachos, Microkinetic Modeling and Reduced Rate Expression of the Water-Gas Shift Reaction on Nickel, *Ind. Eng. Chem. Res.* 57 (31) (2018) 10269–10280.
- M. Maestri, D. Vlachos, A. Beretta, G. Groppi, E. Tronconi, Steam and dry reforming of methane on Rh: Microkinetic analysis and hierarchy of kinetic models, *J. Catal.* 259 (2) (2008) 211–222.
- A.J. Medford, C. Shi, M.J. Hoffmann, A.C. Lausche, S.R. Fitzgibbon, T. Bligaard, J. K. Nørskov, CatMAP: A Software Package for Descriptor-Based Microkinetic Mapping of Catalytic Trends, *Catal. Lett.* 145 (3) (2015) 794–807.
- C.T. Campbell, The Degree of Rate Control: A Powerful Tool for Catalysis Research, *ACS Catal.* 7 (4) (2017) 2770–2779.
- S. Shambhawi, G. Csányi, A.A. Lapkin, Active Learning Training Strategy for Predicting O Adsorption Free Energy on Perovskite Catalysts using Inexpensive Catalyst Features, *Chemistry-Methods* 1 (10) (2021) 444–450.
- O. Mohan, S. Shambhawi, R. Xu, A.A. Lapkin, S.H. Mushrif, Investigating CO<sub>2</sub> Methanation on Ni and Ru: DFT Assisted Microkinetic Analysis, *ChemCatChem* 13 (10) (2021) 2420–2433.
- O. Mohan, Shambhawi, A.A. Lapkin, S.H. Mushrif, Investigating methane dry reforming on Ni and B promoted Ni surfaces: DFT assisted microkinetic analysis and addressing the coking problem, *Cat. Sci. Technol.* 10 (19) (2020) 6628–6643.
- V.A. Tsipourari, X.E. Verykios, Carbon and Oxygen Reaction Pathways of CO<sub>2</sub> Reforming of Methane over Ni/La<sub>2</sub>O<sub>3</sub> and Ni/Al<sub>2</sub>O<sub>3</sub> Catalysts Studied by Isotopic Tracing Techniques, *J. Catal.* 187 (1) (1999) 85–94.
- J. Wei, E. Iglesia, Isotopic and kinetic assessment of the mechanism of reactions of CH<sub>4</sub> with CO<sub>2</sub> or H<sub>2</sub>O to form synthesis gas and carbon on nickel catalysts, *J. Catal.* 224 (2) (2004) 370–383.
- J. Happel, et al., Multiple isotope tracing of methanation over nickel catalyst, *J. Catal.* 65 (1) (1980) 59–77.
- X.E. Verykios, Catalytic dry reforming of natural gas for the production of chemicals and hydrogen, *Int. J. Hydrogen Energy* 28 (10) (2003) 1045–1063.
- D. Qin, D. Xie, H. Zheng, Z. Li, J. Tang, Z. Wei, In-Situ FTIR Study of CO<sub>2</sub> Adsorption and Methanation Mechanism Over Bimetallic Catalyst at Low Temperature, *Catal. Lett.* 151 (10) (2021) 2894–2905.
- L. Foppa, M.-C. Silaghi, K. Larmier, A. Comas-Vives, Intrinsic reactivity of Ni, Pd and Pt surfaces in dry reforming and competitive reactions: Insights from first principles calculations and microkinetic modeling simulations, *J. Catal.* 343 (2016) 196–207.
- W. Zhen, F. Gao, B. Tian, P. Ding, Y. Deng, Z. Li, H. Gao, G. Lu, Enhancing activity for carbon dioxide methanation by encapsulating (111) facet Ni particle in metal–organic frameworks at low temperature, *J. Catal.* 348 (2017) 200–211.
- D.M. Lepore, C. Barratt, P.M. Schwartz, Computational models of chemical systems inspired by Braess' paradox, *J. Math. Chem.* 49 (2) (2011) 356–370.
- F. Abild-Pedersen, J. Greeley, F. Studt, J. Rossmeisl, T.R. Munter, P.G. Moses, E. Skúlason, T. Bligaard, J.K. Nørskov, Scaling Properties of Adsorption Energies for Hydrogen-Containing Molecules on Transition-Metal Surfaces, *Phys. Rev. Lett.* 99 (1) (2007), 016105.
- F. Calle-Vallejo, D. Loffreda, M.T.M. Koper, P. Sautet, Introducing structural sensitivity into adsorption–energy scaling relations by means of coordination numbers, *Nat. Chem.* 7 (5) (2015) 403–410.
- M.M. Montemore, J.W. Medlin, Scaling relations between adsorption energies for computational screening and design of catalysts, *Cat. Sci. Technol.* 4 (11) (2014) 3748–3761.
- C. Fan, Y.-A. Zhu, M.-L. Yang, Z.-J. Sui, X.-G. Zhou, D.e. Chen, Density Functional Theory-Assisted Microkinetic Analysis of Methane Dry Reforming on Ni Catalyst, *Ind. Eng. Chem. Res.* 54 (22) (2015) 5901–5913.
- Z. Xie, Q. Liao, M. Liu, Z. Yang, L.I. Zhang, Micro-kinetic modeling study of dry reforming of methane over the Ni-based catalyst, *Energ. Conver. Manage.* 153 (2017) 526–537.
- S. Chen, J. Zaffran, B. Yang, Descriptor Design in the Computational Screening of Ni-Based Catalysts with Balanced Activity and Stability for Dry Reforming of Methane Reaction, *ACS Catal.* 10 (5) (2020) 3074–3083.
- H. Sun, J. Wu, D. Ma, J. Long, Spatial distribution complexities of traffic congestion and bottlenecks in different network topologies, *App. Math. Model.* 38 (2) (2014) 496–505.
- D. Braess, A. Nagurney, T. Wakolbinger, On a Paradox of Traffic Planning, *Transp. Sci.* 39 (4) (2005) 446–450.
- O.O. Mizrak, N. Ozalp, Fractional analog of a chemical system inspired by Braess' paradox, *Comput. Appl. Math.* 37 (3) (2018) 2503–2518.